

铈离子掺杂对掺镱 SiO₂ 微球自激拉曼激光的增强黄衍堂^{1,2*}, 林晟¹, 刘锦萍¹, 许灿华¹, 廖廷俤^{2**}¹福州大学物理与信息工程学院, 福建 福州 350108;²泉州师范学院光子技术研究中心, 福建 泉州 362000

摘要 受激拉曼散射是拓展激光波长的一种方法。微球腔回音壁模(WGMs)具有模式体积小、功率密度高的特点,有利于研究受激拉曼散射现象。光学介质的极化率大,拉曼增益因子也大,因此通过溶胶-凝胶法在 SiO₂ 微球腔表面共掺杂稀土离子 Yb³⁺ 及重金属离子 Zr⁴⁺,以增加膜层极化率的方式增强拉曼增益,获得阈值降低、效率增加的自激发拉曼激光。对比了在 976 nm 光源激励下 SiO₂ 微球腔分别单掺 Yb³⁺ 与 Yb³⁺-Zr⁴⁺ 离子共掺所产生的 1295 nm 附近三级自激发拉曼激光,结果表明随着 Zr⁴⁺ 离子掺杂浓度提升至 10%,三阶自激发拉曼激光的阈值从 129.47 mW 降低至 15.70 mW,拉曼激光转换效率提升了 3.09 倍,在相同泵浦功率下获得增强的自激发拉曼激光。

关键词 激光技术; 铈/铈共掺杂微球; 高品质因子; 拉曼增益因子; 自激发拉曼激光

中图分类号 O437

文献标志码 A

doi: 10.3788/CJL202148.2401001

1 引言

自激发拉曼激光是一种泵浦光激励增益介质,受激辐射产生基频激光,进而基频激光在介质传输,因受激散射而产生频移的拉曼激光的现象。受激拉曼散射是拓展激光波长的一种重要手段。高功率密度光源泵浦拉曼活性介质所产生的受激拉曼散射能产生一阶以上的级联的受激拉曼散射,使激光波长以介质的拉曼频移为间隔拓展,获得线宽较窄的新波长激光。固体拉曼活性介质有钒酸盐(如 YVO₄)^[1]、钼酸盐(如 PbWO₄)^[2] 等晶体或玻璃材料^[3-4]。当这些拉曼活性介质掺杂了稀土离子时,可作为受激辐射的增益材料,在强泵浦光激励下既可产生受激辐射的基频激光,又可以实现基频激光拉曼频移,即实现自激发拉曼激光输出,如 Nd:GdVO₄^[5]、Nd:PbWO₄^[6]、ZnWO₄^[7] 等。徐瑾瑾等^[8]通过 KTA 晶体与 Nd³⁺:YAG 谐振腔完成了可在 1106.08~1116.62 nm 不连续调谐的自激发拉曼激光器。任席奎等^[9-10]搭建了基于 ZnWO₄/Nd:YAG 的拉曼激光器并获得 1177.6 nm 的一阶斯托克斯激光输出和 1318.3 nm 的二阶斯托克斯激光

输出。赵辉等^[11]基于 Yb³⁺:YAG/Cr⁴⁺:YAG/YAG 键合晶体通过被动调 Q 获得 578.56 nm 黄光输出。自激发拉曼激光器减少了激光腔内的光学元件,使激光器的结构紧凑,进而减少了腔内损耗,提高了激光器的效率,也使得性能更稳定。

近年来,熔融液体表面张力形成的介质微腔由于具有很高的品质因子(可达 10⁹),光波在其中以倏逝场传播时形成一种具有小模式体积(约 300λ³)、高能量密度(约 1 GW/cm²)的回音壁模(WGM),而被广泛用于基础物理与应用研究中^[12],如稀土离子掺杂低阈值光学微腔激光器^[13-14]、低阈值多级拉曼激光器^[15-16]以及微腔传感器^[17-18]等领域。Vahala 课题组^[19]报道了采用硅片上的 SiO₂ 微芯环形腔,在泵浦波长 1561 nm 处获得了高达 2.5×10⁷ 的 Q 值,在泵浦功率 640 μW 的情况下获得 1679 nm 的拉曼激光;采用锥球耦合系统从理论和实验两方面研究了级联受激拉曼散射的阈值和效率、转换效率对 Q 值的依赖性和耦合情况对低阈值拉曼激光的影响^[18,20];采用高 Q 值 SiO₂ 微球在 980 nm 附近获得五阶级联拉曼散射,最高延展至 1231 nm^[15-16]。

收稿日期: 2021-02-21; 修回日期: 2021-04-11; 录用日期: 2021-05-24

基金项目: 福建省科技厅项目(2020Y4005)、福州市科技局项目(2020-GX-14)、闽都创新实验室项目(2021ZR141)

通信作者: *huangyantang@fzu.edu.cn; **tingdi_liao@qztc.edu.cn

同时,对比稀土离子掺杂晶体的自激发拉曼激光现象,黄衍堂等^[21-23]报道了采用锥光纤将 808 nm 的激光耦合入 Nd³⁺ 离子掺杂的高 Q 值 SiO₂ 微球,激发产生了 1080~1097 nm 波段基频激光和波长为 1120~1143 nm 一级自受激拉曼激光。为增强拉曼激光,在微腔外层镀重金属敏化离子掺杂的 SiO₂ 膜层,如掺 Ti⁴⁺^[24]、Zr⁴⁺^[25-26]、Nb⁵⁺^[27] 等,一方面因离子极化率增加而增强拉曼因子,另一方面重金属离子掺杂的膜层折射率增加而增强了对回廊模的聚集,导致功率密度的增加。这两方面的共同效应降低了镀膜 SiO₂ 微腔拉曼激光阈值和增强微腔的拉曼激光,微腔的拉曼激光性能明显改善。

为增强自激发拉曼激光,本文通过溶胶凝胶法对二氧化硅微球腔镀 Yb³⁺-Zr⁴⁺ 共掺杂功能薄膜,研究基于微球腔的自激发拉曼激光增强,本成果一方面产生了可用于第二生物窗口的 1.2~1.3 μm 波段激光,另一方面可为产生高效率自激发拉曼光的材料制备提供参考。

2 基本原理

2.1 材料的极化强度与拉曼增益系数

玻璃的三阶非线性光学性质在很大程度上取决于在玻璃中掺杂形成网络的阴阳离子键的极化率,并且与离子的掺杂浓度有着比较大的关联性^[28]。已报道通过超瑞利光散射法计算了 SiO₂ 和 ZrO₂ 的极化率可以证实系统的极化率取决于粒径和浓度^[29]。SiO₂ 材质通常约在 500 cm⁻¹ 和 1000 cm⁻¹ 处显示出两个不同的拉曼响应峰^[30],分别代表弯曲模式和拉伸模式的拉曼截面 A500 和 A1000,拉曼增益系数与这二者之间的比值 A500/A1000 正相关。在 SiO₂ 溶胶中掺杂 Zr 元素会改变 Si—O 键的性质并影响 O 元素的电荷分布,从而影响弯曲模式和拉伸模式的拉曼截面,增大 SiO₂ 膜层的 A500/A1000 比值,导致极化强度和拉曼增益因子同时增大^[25,30]。体材料的本征拉曼增益因子 g_R 可以表示为^[18,31-33]

$$g_R = \frac{4\pi^2 M c^2}{\hbar \omega_s^2 \omega_p n_s^2} \left(\frac{\partial^2 \sigma}{\partial \omega \partial \Omega} \right), \quad (1)$$

式中: M 为分子数密度; c 是真空中光速;下标 S 和 P 分别示信号光和泵浦光; ω_s 和 ω_p 分别是斯托克斯光和泵浦光的频率; n_s 是微球介质的折射率; $\frac{\partial^2 \sigma}{\partial \omega \partial \Omega}$ 是拉曼截面 σ 分别对斯托克斯光频率附近的频域 ω 和立体角 Ω 偏微分^[33],得到

$$\frac{\partial^2 \sigma}{\partial \omega \partial \Omega} = \frac{\partial \left(\frac{\sigma}{\Delta \omega} \right)}{\partial \Omega} = \frac{1}{\Delta \omega} \frac{\partial \sigma}{\partial \Omega}, \quad (2)$$

式中: $\Delta \omega$ 是频率增量。散射截面对立体角的偏微分定义为单位体积散射介质斯托克斯光子通量与泵浦光子通量的比值:

$$\frac{\partial \sigma}{\partial \Omega} = \frac{N_s}{N_p}. \quad (3)$$

光子通量与电磁波振幅 E 之间的关系可表示为

$$N = \frac{2k}{\hbar \mu_0 \omega^2} |E(\omega)|^2, \quad (4)$$

式中: k 为波矢量大小; \hbar 是常数; μ_0 为磁导率。由(3)、(4)式可得:

$$\frac{\partial \sigma}{\partial \Omega} = \frac{\frac{2k_s}{\hbar \mu_0 \omega_s^2} |E(\omega_s)|^2}{\frac{2k_p}{\hbar \mu_0 \omega_p^2} |E(\omega_p)|^2} = \frac{\frac{2k_s}{\hbar \mu_0 \omega_s^2} |E_s|^2}{\frac{2k_p}{\hbar \mu_0 \omega_p^2} |E_p|^2}. \quad (5)$$

斯托克斯光与泵浦光满足三阶极化耦合方程:

$$\frac{dE_s}{dz} = \frac{3i\omega_s^2}{k_s c^2} \chi^{(3)} |E_p|^2 E_s, \quad (6)$$

$$E_s = E_{s,0} \exp \left[\frac{3i\omega_s^2}{k_s c^2} \chi^{(3)} |E_p|^2 z \right]. \quad (7)$$

将三阶极化率 $\chi^{(3)}$ 分解为实部与虚部之和 $\chi^{(3)} = \chi_R + i\chi_I$,当发生拉曼散射时,虚部 χ_I 恒小于零,且绝对值随极化率增加而增大,则斯托克斯光场可分解为相位调制项和强度变化项的乘积:

$$E_s = E_{s,0} \exp \left(\frac{3i\omega_s^2}{k_s c^2} \chi_R |E_p|^2 z \right) \exp \left(- \frac{3\omega_s^2}{k_s c^2} \chi_I |E_p|^2 z \right), \quad (8)$$

$$|E_s|^2 = E_{s,0}^2 \exp \left(- \frac{6\omega_s^2}{k_s c^2} \chi_I |E_p|^2 z \right). \quad (9)$$

联立(1)、(2)、(5)、(9)式可得:

$$g_R = \frac{4k_s \pi^2 N c^2 E_{s,0}^2 \exp \left(- \frac{6\omega_s^2}{k_s c^2} \chi_I |E_p|^2 z \right)}{\hbar k_p \Delta \omega \omega_s^4 n_s^2 |E_p|^2}. \quad (10)$$

由(10)式可知,虽然折射率增大会减弱拉曼增益,但极化率增加能增大拉曼增益因子。

2.2 微腔拉曼阈值

微球腔的拉曼阈值 P_{th} 的定义^[30]为

$$P_{th} = \frac{\beta n_{eff}^2 V_m}{\lambda_p \lambda_R g_R Q^2}, \quad (11)$$

式中: β 是与锥光纤与微球耦合模场参数相关的常

数; n_{eff} 是有效折射率; V_m 是回廊模的模式体积; λ_p 和 λ_R 分别是泵浦波长和拉曼波长。由(11)式可知, 重金属氧化物掺杂增加 n_{eff} 使拉曼阈值增加, 但能更大地增加 g_R , 减小模式体积 V_m 能减小阈值功率。

利用溶胶凝胶方法^[34]将单掺 Yb^{3+} 和共掺 $\text{Yb}^{3+}-\text{Zr}^{4+}$ 离子膜层粘涂在微球腔表面。镀 $\text{Yb}^{3+}-\text{Zr}^{4+}$ 离子掺杂的膜层, 一方面通过增加极化率使拉曼增益系数 g_R 增大, 另一方面掺 Zr^{4+} 的 SiO_2 膜层折射率 n_{eff} 增大, 微球这层高折射率的膜层使大部分 WGM 光场约束在其中^[35], 改变了 WGM 模场分布方式, 将光场向膜层中聚焦, 减小光学模式体积^[25], 提高了 WGM 功率密度, 二者都有利于降低拉曼激光阈值, 有利于自激发拉曼激光的产生。

3 微球制备及实验装置与测试

3.1 微球功能膜层制备及实验装置

采用标准通信光纤去除涂覆层后在酒精灯火焰上加热成光纤锥, 用电极放电电弧熔融光纤锥末端,

烧制成带柄的 SiO_2 微球备用。选用硝酸镱五水合物 $\text{Yb}(\text{NO}_3)_3 \cdot 5\text{H}_2\text{O}$ 、 $\text{Zr}(\text{NO}_3)_4 \cdot 5\text{H}_2\text{O}$ 分别作为 Yb^{3+} 、 Zr^{4+} 离子提供试剂。用溶胶凝胶法制备 $\text{Yb}^{3+}-\text{Zr}^{4+}$ 掺杂的二氧化硅凝胶, 采用浸入提拉法在 SiO_2 微球表面镀溶胶-凝胶膜, 风干后采用电极放电火花熔融膜层使之致密光滑, 以提高镀膜微球腔的 Q 值。掺杂的 Yb^{3+} 离子浓度(摩尔分数)固定为 4%^[23], 作为对比 Zr^{4+} 离子掺杂浓度分别为 0%、5%、10%, 实验证明三种掺杂浓度中, Zr^{4+} 离子掺杂浓度为 10%(当硝酸镱提供的 Zr^{4+} 离子大于 10% 时, 凝胶容易固化)时具有最高的拉曼增益, 因此将其与掺杂浓度 0% 的情况进行比较。

实验装置如图 1 所示, 用 976 nm 半导体激光器作为泵浦源, 通过双锥光纤与微球腔相切耦合^[26,30,36]将泵浦光耦合入微球内表面形成回廊模, 锥光纤与微球的耦合通过三维调整架调节, 并用显微 CCD 监视。锥光纤的输出端接入光谱分析仪(OA, 600~1700 nm), 测试微球透射输出的光谱。

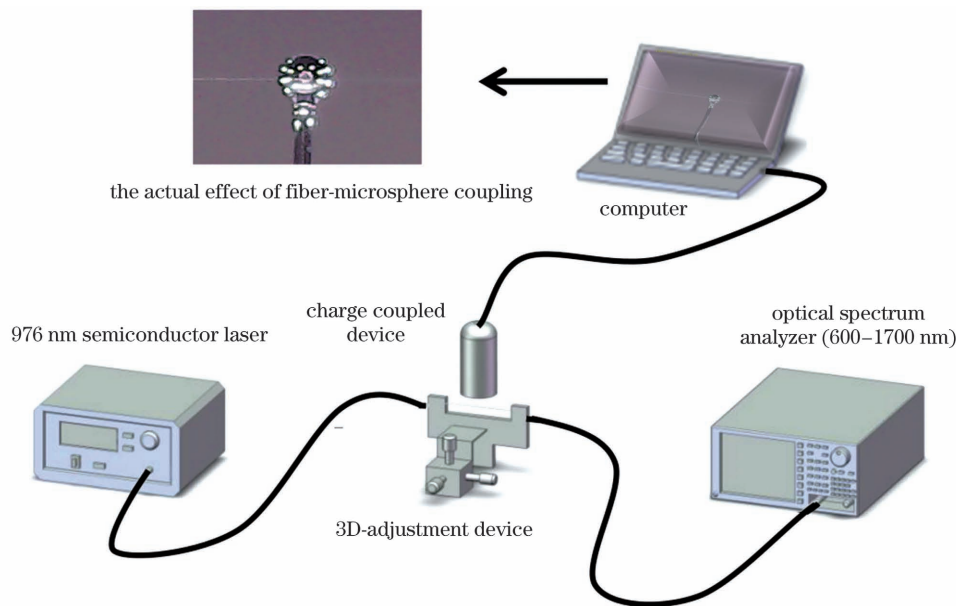


图 1 实验装置示意图

Fig. 1 Schematic diagram of experimental setup

3.2 微球膜层折射率估测

将图 1 中的光源替换为放大自发辐射(ASE)光源, 可以在光谱分析仪上测到如图 2 所示的经锥光纤微球耦合的微球谐振吸收透射谱, 输出光谱中的每一个透射谱吸收峰对应微球腔的一个 WGM。谐振光谱中两个相邻谐振吸收峰的频率或者波长间隔称为自由光谱范围($\Delta\lambda_{\text{FSR}}$), 谐振腔的自由光谱范围与微腔半径 R 、折射率 n_s 满足关系式^[37-39]

$$\Delta\lambda_{\text{FSR}} = \lambda_\nu - \lambda_{\nu+1} = \frac{2\pi n_s R}{\nu} - \frac{2\pi n_s R}{\nu+1} = \frac{2\pi n_s R}{\nu(\nu+1)} \approx \frac{\lambda_\nu^2}{2\pi n_s R}, \quad (12)$$

$$n_s \approx \frac{\lambda_\nu^2}{2\pi \Delta\lambda_{\text{FSR}} R}, \quad (13)$$

式中: λ_ν 、 $\lambda_{\nu+1}$ 是相邻的谐振波长; R 是微球腔的半径。虽然折射率是与波长相关的参数, 但在实验涉及的波长范围内, 其变化量远小于 Zr^{4+} 掺杂导致的

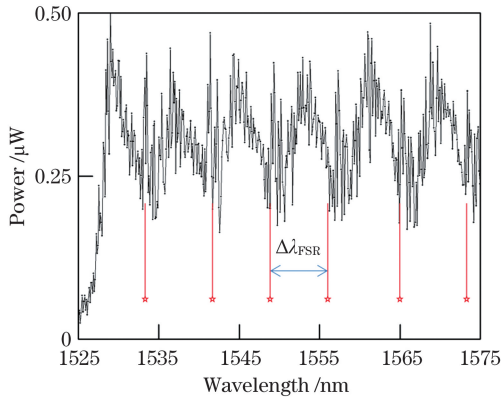


图 2 以 1550 nm ASE 光源为泵浦源锥光纤耦合输出的微球谐振吸收谱
Fig. 2 Resonance absorption spectra of microspheres coupled out of tapered fiber with 1550 nm ASE light source as pump source

折射率变化,因此在讨论中将其视为仅随掺杂浓度变化的参数,并以 ASE 透射光谱测得的 $\Delta\lambda_{\text{FSR}}$ 计算得到的折射率平均值作为该浓度下实验波长范围的折射率。

根据测量结果计算,可得单独掺杂 Yb^{3+} 离子的微球膜层折射率约为 1.482,而 $\text{Yb}^{3+}-\text{Zr}^{4+}$ 共掺微球膜层折射率约为 1.521。折射率的增加是由于 ZrO_2 的折射率高于 SiO_2 ($n_{\text{ZrO}_2} = 2.208, n_{\text{SiO}_2} =$

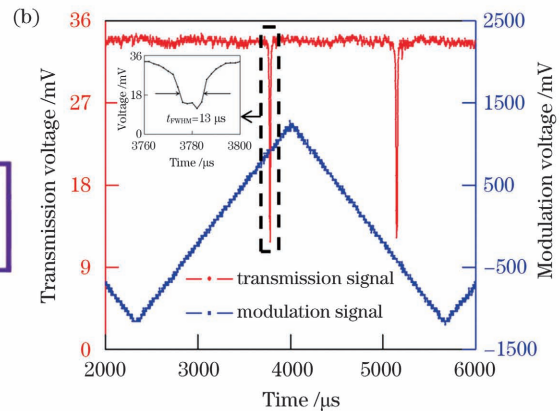
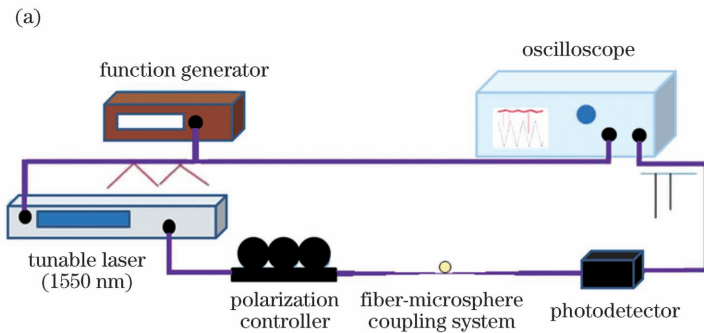


图 3 Q 值测试图。(a)Q 值测试装置示意图;(b)示波器显示图

Fig. 3 Schematic of Q factor testing. (a) Schematic of Q factor test setup; (b) oscilloscope display

将测量结果(对于单掺 Yb^{3+} 微球腔, $\lambda_v = 1521.541 \text{ nm}, U_{\text{single}} = 2400 \text{ mV}, T_{\text{single}} = 3376 \mu\text{s}, t_{\text{FWHM}} = 9 \mu\text{s}$; 对于 $\text{Yb}^{3+}-\text{Zr}^{4+}$ 共掺微球腔, $\lambda_v = 1521.290 \text{ nm}, U_{\text{single}} = 2480 \text{ mV}, T_{\text{single}} = 3360 \mu\text{s}, t_{\text{FWHM}} = 13 \mu\text{s}$)代入计算,单掺 Yb^{3+} 离子的微球腔 Q 值约为 5.14×10^7 ,而 $\text{Yb}^{3+}-\text{Zr}^{4+}$ 共掺微球腔 Q 值约为 3.43×10^7 。虽然掺入了 Zr 元素 SiO_2 溶胶有着比普通更高的固有拉曼增益因子 g_R ,但是 Zr 元素的掺杂会导致品质因子 Q 的下降,这是由于掺

杂离子导致的材料吸收损耗增加。然而,微球腔的 Q 值仍超过 10^7 。对于制备好的锥与微球腔,通常将其用于干燥盒保护,以避免灰尘和水分子附着在微球腔表面导致 Q 值下降。

3.3 微球腔品质因子测量

光学微球腔中的品质因子可以通过谐振峰的谱线宽度来计算,定义为谐振波长 λ_v 与谐振谱线宽 $\Delta\lambda_v$ 的比值为 $Q = \frac{\lambda_v}{\Delta\lambda_v}$ 。

Q 值测量方法如图 3 所示,图中函数发生器输出的三角波调制电信号,一路加到可调谐激光器的 Mod 口驱动压电陶瓷(PZT)围绕某一谐振波长调制扫频,另一分路接示波器 CH1;锥光纤经过微球后输出光接入光电探测器,转换电信号后连接到示波器 CH2 上。通过谐振时产生的谐振吸收下降峰寻找微球腔的固有谐振频率,同时计算微腔 Q 值,其计算公式为

$$Q = \frac{f}{\Delta f} = \frac{\frac{c}{\lambda_v}}{\frac{t_{\text{FWHM}}}{0.5 T_{\text{single}}} \times 300 \times U_{\text{single}}}, \quad (14)$$

式中: f 是微球谐振频率(对应微球的谐振波长 λ_v); Δf 是谐振峰的半峰全宽; t_{FWHM} 为对应于共振吸收下降峰半峰全宽的时间; U_{single} 和 T_{single} 分别为函数发生器输出的三角波峰-峰电压和信号周期。

杂离子导致的材料吸收损耗增加。然而,微球腔的 Q 值仍超过 10^7 。对于制备好的锥与微球腔,通常将其用于干燥盒保护,以避免灰尘和水分子附着在微球腔表面导致 Q 值下降。

4 联级自激发拉曼激光及结果分析

4.1 基频激光与三阶自激发拉曼激光

采用锥球耦合系统,逐渐增大泵浦功率,测试了 Yb^{3+} 单掺与 $\text{Yb}^{3+}-\text{Zr}^{4+}$ 共掺微球的基频激光与自

激发拉曼激光。实验采用直径同为 $68\ \mu\text{m}$ 、膜层厚度约为 $0.5\ \mu\text{m}$ 的单掺 Yb^{3+} 和 $\text{Yb}^{3+}\text{-Zr}^{4+}$ 共掺微球。在相同的泵浦波长 ($976\ \text{nm}$) 和不同

($24.3\ \text{dBm}$) 及相同 ($18.5\ \text{dBm}$) 泵浦功率, 可以观察到对照组的基频激光和自激发拉曼激光光谱如图 4 所示。

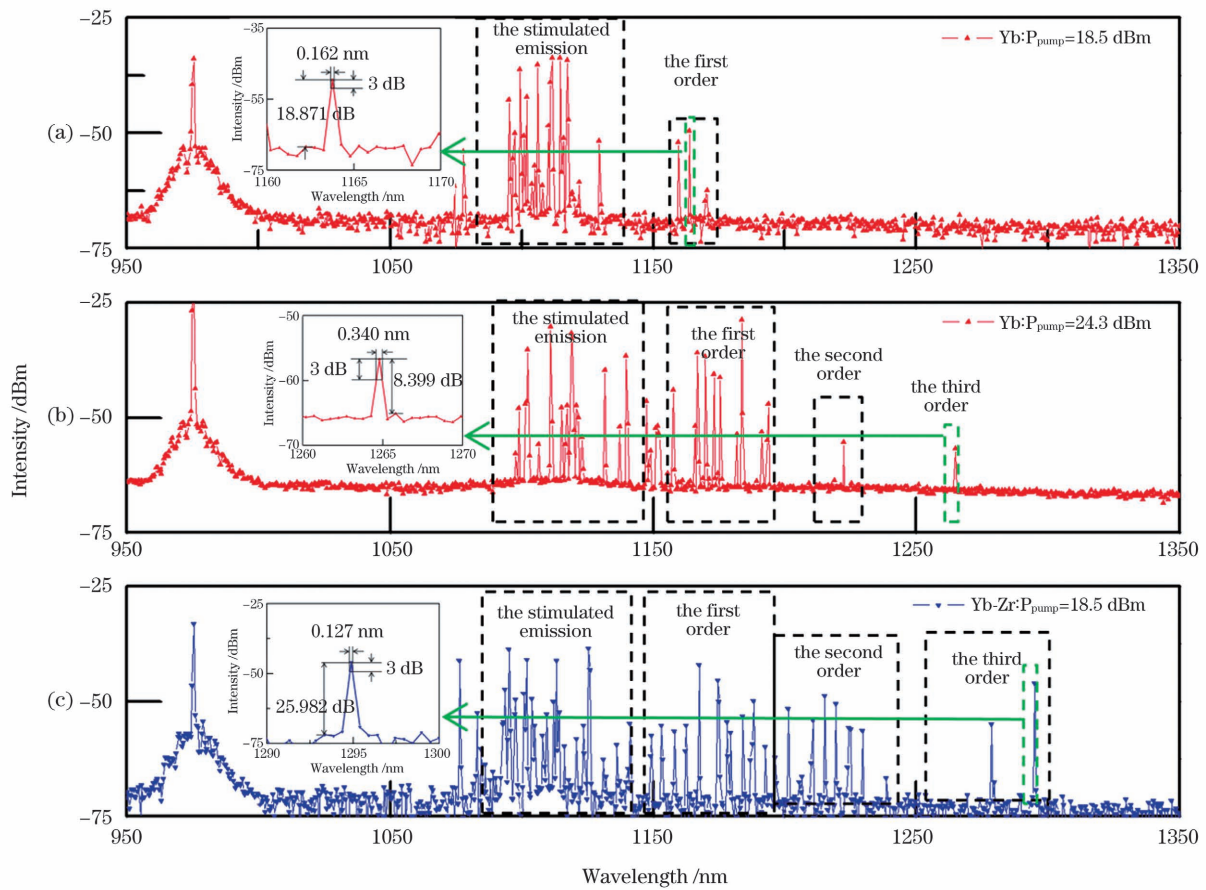


图 4 在 $976\ \text{nm}$ 激光泵浦下 Yb^{3+} 单掺与 $\text{Yb}^{3+}\text{-Zr}^{4+}$ 共掺微球自激发拉曼激光光谱(插图:最高阶自激发拉曼激光的局部细节图)。(a) 泵浦功率为 $18.5\ \text{dBm}$ 时 Yb^{3+} 单掺 SiO_2 微球腔一阶自激发拉曼激光光谱;(b) 泵浦功率为 $24.3\ \text{dBm}$ 时 Yb^{3+} 单掺 SiO_2 微球腔三阶自激发拉曼激光光谱;(c) 泵浦功率为 $18.5\ \text{dBm}$ 时 $\text{Yb}^{3+}\text{-Zr}^{4+}$ 共掺 SiO_2 微球腔三阶自激发拉曼激光光谱, 第三阶激光波长为 $1295\ \text{nm}$

Fig. 4 Yb^{3+} doped and $\text{Yb}^{3+}\text{-Zr}^{4+}$ co-doped self-stimulated Raman scattering spectrum under same pump wavelength but different pump powers (inset: a partial detail view of the highest order self-stimulated Raman scattering laser). (a) First-order self-stimulated Raman output spectrum of Yb^{3+} doped microsphere obtained under pump power of $18.5\ \text{dBm}$; (b) third-order self-stimulated Raman output spectrum of Yb^{3+} doped microsphere under pump power of $24.3\ \text{dBm}$; (c) third-order self-stimulated Raman spectrum of $\text{Yb}^{3+}\text{-Zr}^{4+}$ co-doped microsphere under pump power of $18.5\ \text{dBm}$, with third-order wavelength of $1295\ \text{nm}$

图 4 结果表明, 在相同泵浦功率下, $\text{Yb}^{3+}\text{-Zr}^{4+}$ 共掺的微球腔能够获得三阶级联自激发拉曼激光, 第三级自激发拉曼激光波长到达 $1295\ \text{nm}$, 表明 Zr^{4+} 掺杂能够增强自激发拉曼激光。同时, 在增加泵浦功率的情况下, 也获得了单独掺杂 Yb^{3+} 离子的微球腔三阶级联自激发拉曼激光, 此时泵浦功率为 $24.3\ \text{dBm}$ 。测试过程中, 在同样的泵浦条件和耦合条件下, 多次扫描测得的谱线基本重合, 仅有较小差异。存在差异是由于空气环境中, 气流、温度、湿度

对泵浦光耦合效率产生的影响所致。

4.2 自激发拉曼激光阈值及泵浦光的转换效率

按图 1 实验装置, 逐渐增加泵浦光功率, 依次保存微球输出的透射谱, 记录耦合入微球形成回廊模的泵浦功率以及单掺 Yb^{3+} 与 $\text{Yb}^{3+}\text{-Zr}^{4+}$ 共掺微球产生的三阶自激发级联拉曼激光功率, 如图 5 所示。

图 5 为单掺 Yb^{3+} 与 $\text{Yb}^{3+}\text{-Zr}^{4+}$ 共掺微球所能达到的最高阶自激发拉曼激光(三阶)的激光转换斜率效率和激光阈值。耦合功率及激光强度是通过光

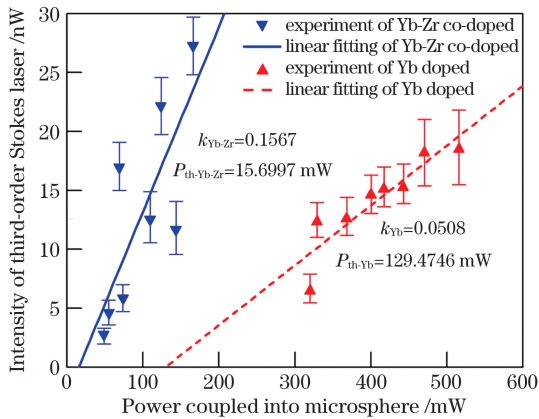


图 5 掺 Yb³⁺ 和 Yb³⁺-Zr⁴⁺ 共掺微球的三阶斯托克斯激光阈值及斜率效率对比

Fig. 5 Comparison of third-order Stokes laser threshold and conversion efficiency of Yb³⁺-doped and Yb³⁺-Zr⁴⁺ co-doped microsphere

谱分析仪和光功率计测量所得出,并通过数据拟合计算出泵浦激光的斜率效率和阈值。图 5 结果表明,摩尔分数 10% 的 Zr⁴⁺ 离子的掺杂使其三阶自激发拉曼激光阈值仅为未掺杂微球腔的 12%,三阶自激发拉曼激光斜率效率则是未掺杂情况的 3.09 倍。自激发拉曼激光效率的提高归因于 Zr⁴⁺ 掺杂使二氧化硅 Si—O 键极化率提高,从而增加了二氧化硅中的声子振动和拉曼增益因子。

4.3 材料拉曼增益系数估算及比较

根据以上测试结果对微球材料掺 Zr⁴⁺ 离子与否的拉曼增益系数进行估算。超高品质因子微腔中 WGM 的有效模式体积通常使用下式近似^[40]

$$V_m = \frac{\int \epsilon(r) E^2(r) d^3r}{[\epsilon(r) E^2(r)]_{\max}} \quad (15)$$

代入微球腔内电磁场各分量可得近似表达式

$$V_m = \begin{cases} 1.02D^{11/6} (\lambda/n)^{7/6}, TE \\ 1.08D^{11/6} (\lambda/n)^{7/6}, TM \end{cases} \quad (16)$$

由(3)式可得拉曼增益因子的近似公式^[40]

$$g_R = \frac{\beta n_{\text{eff}}^2 V_m}{\lambda_p \lambda_R P_{\text{th}} Q^2} \approx \frac{1.02 \beta n_{\text{eff}}^2 D^{11/6} (\lambda/n)^{7/6}}{\lambda_p \lambda_R P_{\text{th}} Q^2}, \quad (17)$$

除 β (与耦合参数相关的常数,在锥光纤相同的情况下,其值近似相等) 以外,式中所有参数都可通过实验确定。由以上测试结果,能够获得摩尔分数 0% 与 10% Zr⁴⁺ 掺杂的拉曼增益因子 g_R 。将实验测得的各参量代入(17)式,计算可得:当溶胶凝胶中 Zr⁴⁺ 的摩尔分数由 0% 增加至 10% 时,以 0% 掺杂的 g_R 为 1,10% 掺杂的 g_R 值增加到 18.97,即实验

结果表明摩尔分数 10% 的 Zr⁴⁺ 掺杂使掺二氧化硅的拉曼增益因子增加了 18.97 倍。

5 结 论

本文采用双锥光纤与高 Q 微球腔耦合系统研究了自激发拉曼激光增强现象。用溶胶-凝胶法和粘涂法在 SiO₂ 微球外层镀上单掺 Yb³⁺ 与 Yb³⁺-Zr⁴⁺ 共掺 SiO₂ 薄膜。理论分析表明,Zr⁴⁺ 离子掺杂的膜层,一方面增加了介质的极化率,从而增大拉曼增益因子 g_R ,另一方面通过增大膜层折射率,使回廊模在膜层聚集,减小了模式体积提高了 WGM 的功率密度,二者都有利于降低拉曼激光阈值、提高自激发拉曼激光效率。对比摩尔分数 0%、5% 和 10% 的 Zr⁴⁺ 掺杂所增强的三阶自激发拉曼增益系数,实验结果表明,当掺杂 Yb³⁺ 的摩尔分数为 4%,Zr⁴⁺ 为 10% 时,与单掺 Yb³⁺ 相比拉曼增益因子增大了约 19 倍,三阶自激发拉曼激光斜率效率增加了 3.09 倍,第三级自激发波长扩展到 1295 nm。Zr⁴⁺ 离子掺杂对掺 Yb³⁺ SiO₂ 微球自激发拉曼激光的增强作用,与理论分析相一致。通过改进 Yb³⁺-Zr⁴⁺ 共掺方法与比例,以及改进微球腔的制备工艺,增加品质因子,有望获得更低阈值、更高阶数的自激发拉曼散射激光。该系统的优势在于结构紧凑、制作简易、重复性好,自激发拉曼激光性能较好。

参 考 文 献

- [1] Chang Y T, Su K W, Chang H L, et al. Compact efficient Q-switched eye-safe laser at 1525 nm with a double-end diffusion-bonded Nd:YVO₄ crystal as a self-Raman medium [J]. Optics Express, 2009, 17 (6): 4330-4335.
- [2] Basiev T T, Doroshenko M E, Smetanin S N, et al. Multi-wave SRS oscillation in PbMoO₄ and PbMo_{0.5}W_{0.5}O₄ crystals under 18 picosecond laser pumping [J]. Laser Physics Letters, 2012, 9 (12): 853-857.
- [3] Chen H T, Lou Q H, Dong J X, et al. High-efficiency 1598.5-nm third Stokes Raman laser based on Barium nitrate crystal [J]. Chinese Optics Letters, 2006, 4(7): 404-406.
- [4] Zhang H N, Chen X H, Wang Q P, et al. Dual-wavelength actively Q-switched diode-end-pumped ceramic Nd:YAG/BaWO₄ Raman laser operating at 1240 and 1376 nm [J]. Laser Physics Letters, 2014, 11(10): 105806.
- [5] Chen Y F, Huang H Y, Lee C C, et al. High-power diode-pumped Nd:GdVO₄/KGW Raman laser at

- 578 nm[J]. *Optics Letters*, 2020, 45(19): 5562-5565.
- [6] Lan R J, Zhang F, Wang Z P, et al. Efficient near-infrared, multiwavelengths PbWO₄ Raman laser[J]. *Optical Engineering*, 2017, 56(9): 096112.
- [7] Ren X K, Xie J, Ruan S C, et al. Diode-end-pumped solid state ZnWO₄ Raman laser at 2254 nm[J]. *Laser Physics*, 2020, 30(1): 015001.
- [8] Xu J J, Zhang X Y, Cong Z H, et al. Tunable Nd³⁺:YAG/KTiOAsO₄ Raman lasers [J]. *Chinese Journal of Lasers*, 2020, 47(6): 0601002.
徐瑾瑾, 张行愚, 丛振华, 等. Nd³⁺:YAG/KTiOAsO₄可调谐拉曼激光器[J]. *中国激光*, 2020, 47(6): 0601002.
- [9] Ren X K, Xie J, Ruan S C, et al. First-Stokes Raman lasers based on ZnWO₄/Nd:YAG [J]. *Chinese Journal of Lasers*, 2020, 47(6): 0601003.
任席奎, 谢建, 阮双琛, 等. 基于 ZnWO₄/Nd:YAG 的一阶斯托克斯拉曼激光器[J]. *中国激光*, 2020, 47(6): 0601003.
- [10] Ren X K, Xie J, Ruan S C, et al. ZnWO₄/Nd:YAG second-order Raman laser at 1318 nm [J]. *Acta Optica Sinica*, 2020, 40(5): 0536001.
任席奎, 谢建, 阮双琛, 等. 1318 nm ZnWO₄/Nd:YAG 二阶拉曼激光器[J]. *光学学报*, 2020, 40(5): 0536001.
- [11] Zhao H, Wang H Y, Zhu S Q, et al. 578.5 nm end-pumped passively Q-switched Raman yellow laser [J]. *Laser & Optoelectronics Progress*, 2021, 58(1): 0114004.
赵辉, 王浩宇, 朱思祁, 等. 578.5 nm 端面泵浦被动调 Q 拉曼黄光激光器[J]. *激光与光电子学进展*, 2021, 58(1): 0114004.
- [12] Wei G Q, Yu Y, Zhuo M P, et al. Organic single-crystalline whispering-gallery mode microlasers with efficient optical gain activated via excited state intramolecular proton transfer luminogens [J]. *Journal of Materials Chemistry C*, 2020, 8(34): 11916-11921.
- [13] Li X J, Wang K Y, Chen M M, et al. Stable whispering gallery mode lasing from solution-processed formamidinium lead bromide perovskite microdisks[J]. *Advanced Optical Materials*, 2020, 8(15): 2000030.
- [14] Fabitha K, Wakiyama Y, Oshima H, et al. Realization of sharp visible WGM lasing from Sm³⁺:ZnO micro-spheres fabricated by laser ablation technique[J]. *Journal of Physics D: Applied Physics*, 2020, 53(13): 135302.
- [15] Zhang P J, Huang Y, Guo C L, et al. Study of cascaded Raman scattering laser in silica microsphere pumped by 976 nm laser[J]. *Acta Physica Sinica*, 2013, 62(22): 224207.
张培进, 黄玉, 郭长磊, 等. 976 nm 激光抽运二氧化硅微球级联拉曼散射激光的研究[J]. *物理学报*, 2013, 62(22): 224207.
- [16] Min B, Kippenberg T J, Vahala K J. Compact, fiber-compatible, cascaded Raman laser [J]. *Optics Letters*, 2003, 28(17): 1507-1509.
- [17] Min B, Kippenberg T J, Yang L, et al. Erbium-implanted high-Q silica toroidal microcavity laser on a silicon chip [J]. *Physical Review A*, 2004, 70(3): 033803.
- [18] Kippenberg T J, Spillane S M, Min B, et al. Theoretical and experimental study of stimulated and cascaded Raman scattering in ultrahigh-Q optical microcavities[J]. *IEEE Journal of Selected Topics in Quantum Electronics*, 2004, 10(5): 1219-1228.
- [19] Yang L, Carmon T, Min B, et al. Erbium-doped and Raman microlasers on a silicon chip fabricated by the sol-gel process[J]. *Applied Physics Letters*, 2005, 86(9): 091114.
- [20] Spillane S M, Kippenberg T J, Vahala K J. Ultralow-threshold Raman laser using a spherical dielectric microcavity[J]. *Nature*, 2002, 415(6872): 621-623.
- [21] Huang Y T, Peng L X, Zhuang S J, et al. Stimulated lasing and self-excited stimulated Raman scattering of Nd³⁺ doped silica microsphere pumped by 808 nm laser[J]. *Acta Physica Sinica*, 2017, 66(24): 244208.
黄衍堂, 彭隆祥, 庄世坚, 等. 掺钕微球的受激辐射激光和自受激拉曼散射[J]. *物理学报*, 2017, 66(24): 244208.
- [22] Wu T J, Huang Y T, Ma J, et al. Study on luminescent properties of Yb³⁺-doped phosphosilicate microsphere[J]. *Acta Physica Sinica*, 2014, 63(21): 217805.
吴天娇, 黄衍堂, 马靖, 等. 掺 Yb³⁺ 磷硅酸盐微球腔发光特性的探究[J]. *物理学报*, 2014, 63(21): 217805.
- [23] Huang Y, Zhang P J, Guo C L, et al. Up-conversion and self-stimulated Raman laser in a codoped microsphere [J]. *IEEE Photonics Technology Letters*, 2013, 25(14): 1385-1388.
- [24] Deka N, Maker A J, Armani A M. Titanium-enhanced Raman microcavity laser [J]. *Optics Letters*, 2014, 39(6): 1354-1357.
- [25] Choi H, Armani A M. High efficiency Raman lasers based on Zr-doped silica hybrid microcavities [J]. *ACS Photonics*, 2016, 3(12): 2383-2388.
- [26] Choi H, Armani A M. Raman-Kerr frequency combs in Zr-doped silica hybrid microresonators[J]. *Optics*

- Letters, 2018, 43(12): 2949-2952.
- [27] Farrow L A, Vogel E M. Raman spectra of phosphate and silicate glasses doped with the cations Ti, Nb and Bi[J]. Journal of Non-Crystalline Solids, 1992, 143: 59-64.
- [28] Irimpan L, Nampoori V P N, Radhakrishnan P, et al. Size-dependent enhancement of nonlinear optical properties in nanocolloids of ZnO [J]. Journal of Applied Physics, 2008, 103(3): 033105.
- [29] Xu W X. Polarizabilities of nanoparticles of SiO₂ and ZrO₂ [J]. Acta Physico-Chimica Sinica, 2007, 23 (11): 1808-1810.
- [30] Colomban P, Slodczyk A. Raman intensity: an important tool in the study of nanomaterials and nanostructures[J]. Acta Physica Polonica A, 2009, 116(1): 7-12.
- [31] Kippenberg T J, Spillane S M, Armani D K, et al. Ultralow-threshold microcavity Raman laser on a microelectronic chip [J]. Optics Letters, 2004, 29 (11): 1224-1226.
- [32] Stolen R H, Ippen E P. Raman gain in glass optical waveguides[J]. Applied Physics Letters, 1973, 22 (6): 276-278.
- [33] Rivero C, Richardson K, Stegeman R, et al. Quantifying Raman gain coefficients in tellurite glasses[J]. Journal of Non-Crystalline Solids, 2004, 345/346: 396-401.
- [34] Coccioli R, Boroditsky M, Yablonovitch E, et al. Smallest possible electromagnetic mode volume in a dielectric cavity [J]. IEE Proceedings-Optoelectronics, 1998, 145(6): 391-397.
- [35] Ostby E P, Yang L, Vahala K J. Ultralow-threshold Yb³⁺:SiO₂ glass laser fabricated by the sol-gel process [J]. Optics Letters, 2007, 32(18): 2650-2652.
- [36] Liu J H, Griebner U, Petrov V, et al. Efficient continuous-wave and Q-switched operation of a diode-pumped Yb:KLu(WO₄)₂ laser with self-Raman conversion[J]. Optics Letters, 2005, 30(18): 2427-2429.
- [37] Guo C L, Huang Y, Zhang P J, et al. Study of laser emission from Er³⁺-doped silica microsphere pumped by 976 nm light [J]. Chinese Journal of Lasers, 2013, 40(3): 0302004.
郭长磊, 黄玉, 张培进, 等. 976 nm 光抽运掺 Er³⁺ 二氧化硅微球产生激光的研究[J]. 中国激光, 2013, 40(3): 0302004.
- [38] Del'Haye P, Arcizet O, Gorodetsky M L, et al. Frequency comb assisted diode laser spectroscopy for measurement of microcavity dispersion [J]. Nature Photonics, 2009, 3(9): 529-533.
- [39] Spillane S M, Kippenberg T J, Painter O J, et al. Ideality in a fiber-taper-coupled microresonator system for application to cavity quantum electrodynamics [J]. Physical Review Letters, 2003, 91(4): 043902.
- [40] Cai M, Painter O, Vahala K J. Observation of critical coupling in a fiber taper to a silica-microsphere whispering-gallery mode system[J]. Physical Review Letters, 2000, 85(1): 74-77.

Self-Stimulated Raman Laser Enhancement of Yb³⁺-Zr⁴⁺ Co-Doped Microspheres

Huang Yantang^{1*}, Lin Sheng¹, Liu Jingping¹, Xu Canxua, Liao Tingdi^{2**}

¹ College of Physics and Information Engineering, Fuzhou University, Fuzhou, Fujian 350116, China;

² Research Center for Photonic Technology, Quanzhou Normal University, Quanzhou, Fujian 362000, China

Abstract

Objective Stimulated Raman scattering is an important method to extend the wavelength of the laser. The self-stimulated Raman laser is a phenomenon of the pump wavelength to excite the ions of the rare-earth-doped laser gain media and generate the fundamental mode, single-frequency laser, which then generates the stimulated Raman scattering laser. The self-stimulated Raman laser reduces the optical elements in the cavity, yielding a compact laser to reduce the optical loss, and improve the performance and efficiency of the laser. Due to the high-quality factor (Q , up to 10^9) of the whispering gallery mode (WGM), the silica microcavity has been widely used in the study of nonlinear optical phenomena. The first-order self-Raman laser for Nd³⁺ doped SiO₂ microspheres with high Q -value has been reported. To enhance the self-Raman laser, the silica microspheres were coated with Yb³⁺-Zr⁴⁺ doped silica film using the sol-gel and immersion method. The 976 nm pump laser was coupled with a tapered optical fiber to form a highpower density WGM in the inner surface of the microspheres. The results provide a reference for the

preparation of materials with a high efficiency self-stimulated Raman laser, allowing the laser to operate at 1.2–1.3 μm wavelength band which can be used in the second near-infrared window.

Methods After removing the coating layer of the standard single mode fiber, the single mode fiber was heated using an alcohol lamp to form the tapered fiber. The end of the tapered fiber was fused with the electrode discharge arc and formed into SiO_2 microspheres with handles for operation. The Yb^{3+} Zr^{4+} doped silica was prepared by the sol-gel method with the Yb^{3+} concentration of 4%, and the doping concentrations of Zr^{4+} were 0%, 5%, 10%, and 15%. The optimal doping concentration of Zr^{4+} was 10%. The sol-gel film was deposited on the surface of SiO_2 microspheres via the immersion-lifting method. After drying, the film was melted using the electrode discharge arc to improve the Q -value of the coated microspheres. A 976 nm semiconductor laser was used as the pump source. Next, the pump light was coupled into the inner surface of the microsphere equator to form WGM by the tapered optical fiber. The coupling position between the tapered optical fiber and the microsphere was controlled by a three-dimensional adjusting frame and monitored by a charge-coupled device microscope. The output end of the tapered fiber was connected to an optical spectral analyzer (OSA, 600–1700 nm) to measure the transmission spectrum of the microspheres (Fig. 1). The basic frequency laser and self-Raman laser of Yb^{3+} -doped and Yb^{3+} - Zr^{4+} co-doped microspheres were measured using this setup by gradually increasing the pump power.

Results and Discussions The Yb^{3+} -doped microsphere and Yb^{3+} - Zr^{4+} co-doped microsphere have the same diameter of 68 μm with the function film thickness of 0.5 μm . Under the 976 nm excited laser with the power of 18.5 dBm, the self-stimulated Raman scattering spectra can be observed. Three orders of the cascade self-stimulated Raman laser were obtained; the wavelength of the third-order self-Raman laser can reach up to 1295 nm (Fig. 4). Alternatively, the Yb^{3+} -doped microsphere obtained three cascade self-Raman lasers with the pump power of 24.3 dBm, which verified that Zr doping can enhance the self-stimulated Raman laser. Thus, the laser conversion efficiency and the threshold of the third-order self-Raman laser can be achieved (Fig. 6). The 10% doping concentration of Zr^{4+} makes the third-order self-Raman laser threshold only 12% of the Yb-doped microsphere, and the conversion efficiency is 3.09 times of Yb^{3+} -doped, which attributes to the improvement of the high polarization of the silica bond by Zr^{4+} doping, thereby increasing the phonon vibration and Raman gain coefficient of the silica. According to the results, the Raman gain coefficient of the microsphere material with and without Zr^{4+} doping is estimated and then compared; the results show that the Yb^{3+} 4% mol/ Zr^{4+} 10% mol doped silica increases the Raman gain factor by 18.966 times compared to the Yb^{3+} 4% mol doped silica.

Conclusions In this study, the phenomenon of the self-stimulated Raman laser enhancement is investigated using a high Q -value microsphere cavity coupled with a tapered optical fiber. The SiO_2 microspheres were coated with Yb^{3+} or $\text{Yb}^{3+}/\text{Zr}^{4+}$ doped SiO_2 thin films via the sol-gel adhesive coating method. Theoretical analysis shows that the Zr^{4+} ion doped films can increase the susceptibility of the rare-earth-doped gain media and increase the Raman gain factor as well as increase the film's refractive index to result in gathering WGMs, thereby reducing the mode volume and increasing the power density of the WGM. Both effects can reduce the Raman laser threshold and improve the efficiency of the self-stimulated Raman laser. When compared with the Yb^{3+} -doped silica microsphere, the experimental results show that the silica microsphere with co-doping concentration of 4% mol $\text{Yb}^{3+}/10$ mol% Zr^{4+} increases the Raman gain coefficient by 19 times, the slope efficiency of the third-order self-stimulated Raman laser increases by 3.09 times, and the third-order self-stimulated wavelength extends to 1295 nm. The enhancement effect of the self-stimulated Raman laser of the $\text{Yb}^{3+}/\text{Zr}^{4+}$ co-doped silica microspheres is consistent with the theoretical analysis.

Key words laser technique; microspherical cavity; whispering gallery mode; ultra-high-quality factor; Raman gain; self-stimulated Raman

OCIS codes 140.3550; 140.3945; 160.5690; 160.6060